RSC Advances

ROYAL SOCIETY OF CHEMISTRY

www.rsc.org/advances

Journal Name

RSCPublishing

ARTICLE

Solvent determines the formation and properties of metal-organic framework

Cite this: DOI: 10.1039/xOxxOOOOOx

Bingxing Zhang, Jianling Zhang*, Chengcheng Liu, Xinxin Sang, Li Peng, Xue Ma, Tianbin Wu, Buxing Han and Guanying Yang

Received 00th January 2012,
Accepted 00th January 2012

DOI: 10.1039/xOxxOOOOOx

www.rsc.org/

The formation of a water-sensitive metal-organic framework (MOF), $Cu_3(BTC)_2$ (BTC=1,3,5-benzenetricarboxylate), in water/ethanol solvent system was studied systematically. The X-ray diffraction results prove that the MOF cannot form in pure water or in the water/ethanol mixture with a small amount of ethanol. As the ethanol content exceeds 30 vol%, the crystallined MOF can be obtained. The scanning electron microscope images of the as-synthesized MOFs show the formation of MOF nanoparticles with average size of 20-300 nm. The MOF particle size is decreased with the increasing ethanol content in the mixed solvent. The FT-IR spectra give further support for the MOF formation in water/ethanol mixtures with ethanol volume ratios higher than 30 vol%. The thermogravimetric analysis shows that the MOF can keep stable up to 300 ^oC. Moreover, FT-IR spectra and thermogravimetric analysis give consistent information on the solvent amount entrapped in the MOF pores. The porosities of the MOFs were determined by N_2 adsorption-desorption method. When the ethanol volume ratio reaches to 75%, the largest S_{BET} value of 1067 m^2g^{-1} and V_t of 0.52 cm^3g^{-1} of the MOF were obtained. The possible mechanism for the MOF formation in water/ethanol solvent system and the dependence of the MOF size on the solvent composition was discussed from the hydrogen bond strength between solvent molecules and ligands in different water/ethanol solvent system.

1. Introduction

Metal-organic framework with controlled morphology and properties have shown application potential in gas adsorption,[1-3] separation,[4] drug release,[5,6] sensing[7] and catalysis,[8-10] owing to their large surface area, relatively mass reactive sites, tunable structure and well-defined porosity. To modulate the structures and properties of the MOFs is of great importance because the applications of the MOFs are dependent on their structures and properties. Up to now, diverse kinds of methods have been proposed for modulating the size, morphology, and properties of MOFs, such as utilizing different solvents,[11,12,13] templating method,[14,15,16] acid-based adjustment route,[17] sonochemical process,[18] etc. Among these routes, solvent adjustment method undoubtedly is the most convenient way to fabricate MOF materials with desirable structures and properties. The conventional solvents for MOF formation are organic liquids, such as N,N-dimethylformamide (DMF), N,N-diethylformamide (DEF), 1-methyl-2-pyrrolidone (NMP). Besides, the binary solvents with water or ethanol (e.g. DMF/ethanol,[19] DMF/water[20]) have been used for the MOF synthesis. Generally, a solvothermal process is needed for the MOF formation and the reaction temperature is usually controlled to be higher than 100 ^oC.

Water is the most environmentally benign, economic and ideal solvent in the world. The hydrothermal process has been reported for the MOF synthesis with many advantages.[21,22] However, it has been known that a majority of MOFs are unstable in aqueous medium, suffering from phase changes, loss in crystallinity, and structural decomposition.[23] Therefore, water is absolutely avoided in the preparation of the water-sensitive MOFs. Recently, Bai[14] group and Kirschhock[15] group have used a mixture of water with ethanol as solvent for the synthesis of $Cu_3(BTC)_2$ (BTC=1,3,5-benzenetricarboxylate), which is one of the most extensively explored MOF for its various use.[24-26] Most interestingly, it gives a clue that the presence of ethanol might prevent the damaging effect of water on $Cu_3(BTC)_2$ and thus the structure integrity of the $Cu_3(BTC)_2$ could be well kept in an aqueous medium. Moreover, this route is much attractive because it can proceed at room temperature and is environmentally benign. Nevertheless, these two papers are focused on the characterization and application of the MOF formed in water/ethanol mixture with a fixed composition (with equal or approximately equal volume of water and ethanol). The fine modulation on size, morphology and properties of the MOF by controlling the solvent composition and the underlying mechanism have not been studied.

Herein, we carried out a systematic investigation on the $Cu_3(BTC)_2$ formation in a series of water/ethanol mixtures with ethanol volume ratios from zero to 100%. It was found that an enough amount of ethanol (>30 vol%) is needed to ensure the formation of $Cu_3(BTC)_2$ MOF in an aqueous medium, i.e. a small amount of ethanol in water does not work for the MOF formation. The $Cu_3(BTC)_2$ nanoparticles with average size of 20-300 nm were obtained and their size and porosity properties can be easily tuned by changing the composition of the mixed solvent. The mechanism for the ethanol-induced MOF formation in an aqueous medium and the downsizing of the MOF particles were discussed from the hydrogen bonding interactions between solvent molecules and organic ligand. This research is meaningful in view of the following points. First, it developed a facile and environmental-friendly route for modulating the size and properties of MOF particles. Second, it provides a new insight into the solvent effect on the MOF formation.

2. Experimental

2.1 Materials

Copper(II) acetate monohydrate ($Cu(OAc)_2 \cdot H_2O$) (A. R. Grade) were obtained from Alfa Aesar. 1,3,5-Benzenetricarboxylic acid (H_3BTC) (purity 95%) were provided by Aldrich. Absolute ethanol and deionized water were provided by Beijing Analysis Instrument Factory. All these materials were used without further purification.

2.2 MOF synthesis

For the MOF synthesis, the mixtures of absolute ethanol and deionized water with different ethanol volume ratios of 0, 25%, 33%, 50%, 67%, 75%, and 100% were prepared. H_3BTC (2.5 mmol) and $Cu(OAc)_2 \cdot H_2O$ (2.5 mmol) were dissolved in water/ethanol mixture (60 mL), respectively. The $Cu(OAc)_2$ solution was dropped into the H_3BTC solution under rapid stirring. After the mixture was stirred for 6 hours at room temperature, the stirrer was stopped. The blue suspension was separated by centrifugation and the precipitate was filtered and washed with water/ethanol for several times. The product was obtained after drying at 60 ^oC under vacuum for 24 hours.

2.3 MOF Characterizations

The morphologies of the as-synthesized MOFs were characterized by scanning electron microscope (SEM, HITACHI S-4800). X-ray diffraction (XRD) was performed on a Rigaku D/max-2500 diffractometer with Cu Kα radiation (λ= 1.5418 Å) at 40 kV and 200 mA. The porosity properties of the MOFs were determined by nitrogen adsorption-desorption isotherms using a Micromeritics ASAP 2020 (M + C) system. The FT-IR spectra were obtained using a Bruker Tensor 27 spectrometer. The thermogravimetric (TG) measurement was carried out using Pyris 1 TGA with N_2 flow of 10 mL/min.

2.4 Solvent effect on H_3BTC molecules

UV-vis spectra of the H_3BTC solutions (3.3×10^{-5} mol/L) in water/ethanol mixtures were determined on a Varian Cary 1E UV-vis spectrophotometer. The spectra were measured at a scanning rate of 1 nm/s.

3. Results and discussion

3.1 XRD characterization

The MOF formation in the water/ethanol mixtures with different ethanol volume ratios were investigated. As shown in Fig. 1, the XRD patterns of the smaples synthesized in pure water and in the water/ethanol mixture with a small amount of ethanol (curves a and b) are completely different from the simulated XRD pattern of HKUST-1 (curve h), which is one of the most widely studied Cu-MOFs.[27-31] The XRD patterns correspond to the collapsed MOF network, exhibing individual carboxyl groups that are not coordinated to Cu atom.[32] It can be attributed to the existence of a large amount of water, which effectively prevents the coordination between carboxyl groups and Cu atom.[33] As the ethanol content is increased to be or higher than 33%, the XRD patterns of the samples (curves c-g) coincide well with the simulated XRD pattern of HKUST-1 (curve h), proving the formation of crystalline $Cu_3(BTC)_2$. The XRD results reveal that a certain amount of ethanol can promote the formation of $Cu_3(BTC)_2$ in an aqueous medium. It is noted that the X-ray diffractions of the MOFs are broadened, indicating that the MOF is composed of small nano-crystallites (curves c-g). Moreover, the diffractions of the MOF synthesized in the water/ethanol mixture with more ethanol are more broadened, indicative of the decreased particle size.

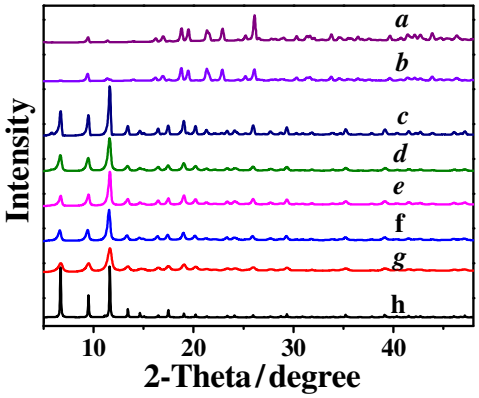

Fig. 1 XRD patterns of the $Cu_3(BTC)_2$ synthesized in water/ethanol mixtures with ethanol volume ratios: (a) 0, (b) 25%, (c) 33%, (d) 50%, (e) 67%, (f) 75%, (g) 100% and the simulated XRD pattern of HKUST-1 (h).

3.2 Morphologies

Fig. 2 shows the SEM images of the MOFs synthesized in water/ethanol mixtures with different ethanol volume ratios. The MOF synthesized in the water/ethanol mixture with ethanol volume ratio 33% presents large crystals in size of 200-400 nm (Fig. 2a). When the volume ratio of ethanol reaches to 50%, the average crystal size of the as-synthesized MOF is sharply reduced to ~60 nm (Fig. 2b). With further increasing the proportion of ethanol, the crystal size gradually decreases (Fig. 2c and 2d). The MOF synthesized in pure ethanol has the smallest particle size of ~20 nm (Fig. 2e). It indicates that the crystal size of the MOFs can be modulated by the composition of water/ethanol mixture. The SEM result is well consistent with the XRD result.

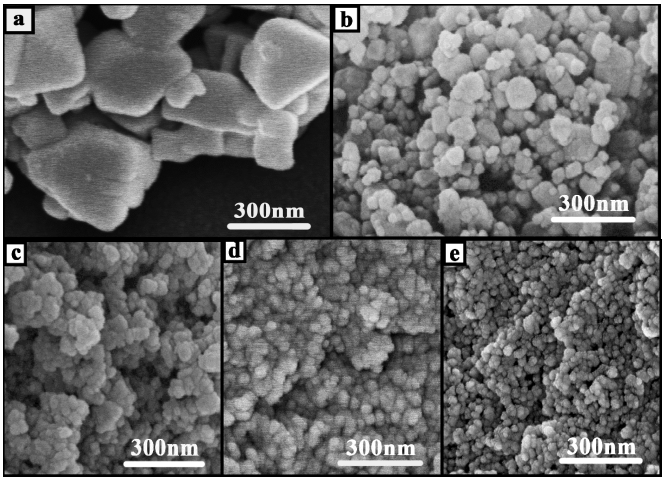

Fig. 2 SEM images of the $Cu_3(BTC)_2$ synthesized in water/ethanol mixtures with ethanol volume ratios of 33% (a), 50% (b), 67% (c), 75% (d) and 100% (e).

3.3 FT-IR spectra

The FT-IR spectra of the five MOFs synthesized in water/ethanol mixtures with different ethanol volume ratios are shown in Fig. 3A. The characteristic asymmetric (1618 cm^{-1}, 1559 cm^{-1}) and symmetric vibration (1442 cm^{-1}, 1374 cm^{-1}) of carboxylate anions in deprotonated H_3BTC are clearly observed (curves a-e). The wavenumber gap between asymmetric and symmetric vibration of carboxylate anions is narrowed, comparing with that of H_3BTC (curve f). It indicates that carboxylate groups of BTC are coordinated to Cu (II) ions.[8,34] A large broad band occurs at about 3400 cm^{-1}, which can be assigned to the stretching vibration of OH group from solvent (water and ethanol) molecules trapped within the MOF pores.[35-37] Obviously, the absorption of the MOF synthesized in water/ethanol mixture with more ethanol moves to higer wavenumber. Fig. 3B shows the dependence of the wavenumber of -OH stretching vibration on ethanol volume ratio, from which the blue shift with the increasing ethanol content can be clearly observed. It indicates that less solvent is entrapped into the pores of the MOF synthesized in the mixture with more ethanol.

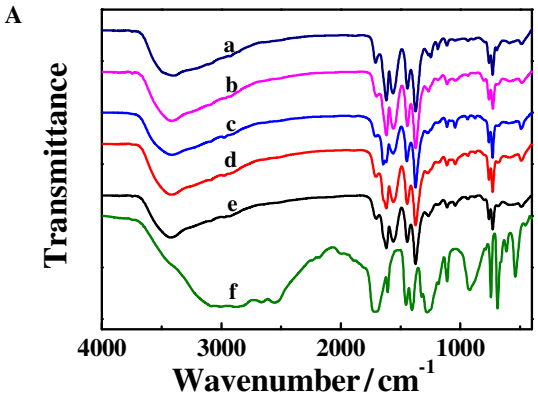

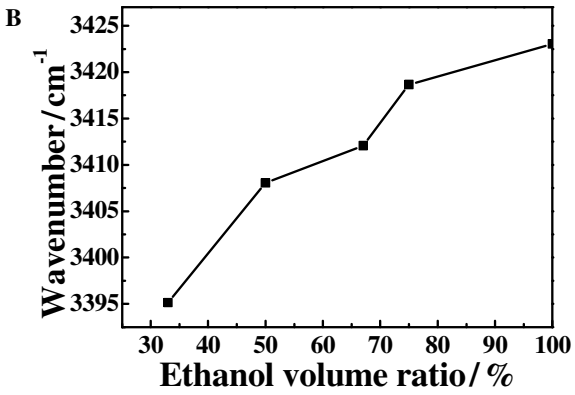

Fig. 3 A: FT-IR spectra of the $Cu_3(BTC)_2$ synthesized in water/ethanol mixtures with ethanol volume ratios of 33% (a), 50% (b), 67% (c), 75% (d) and 100% (e) and H_3BTC (f). B: Dependence of the wavenumber of -OH stretching vibration on ethanol volume ratio.

3.4 Thermogravimetric analysis

Fig. 4 shows the thermogravimetric curves of the $Cu_3(BTC)_2$ synthesized in water/ethanol mixtures with different ethanol volume ratios. The first stage of weight loss (about 3%) in temperature range of 40-100 °C corresponds to the physical desorption of surface adsorbed water and ethanol.[38] The second stage of weight loss occurs in temperature range 100-245 °C, resulting from the desorption of solvent molecules adsorbed in MOF pores. The weight loss is 16.8%, 15%, 11.3%, 10.5%, and 9.5% for the MOFs synthesized in water/ethanol mixtures with ethanol volume ratios of 33%, 50%, 67%, 75% and 100%, respectively. Evidently, the weight loss of adsorbed solvent is less for the MOFs synthesized in the mixture with more ethanol. The TG result is consistent with the FT-IR result that -OH stretching vibration moves to higher wavenumber due to the less amount of solvent entrapped in the MOF pores. As shown in Fig. 4, the third weight loss over 300 °C corresponds to the structural decomposition of $Cu_3(BTC)_2$ to CuO and volatile compounds.[39,40]

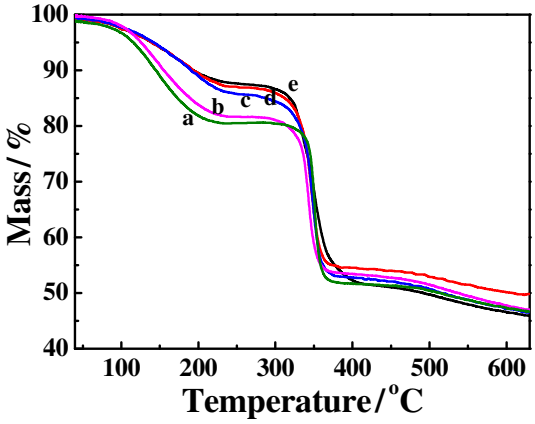

Fig. 4 TG curves of the $Cu_3(BTC)_2$ synthesized in water/ethanol mixtures with ethanol volume ratios of 33% (a), 50% (b), 67% (c), 75% (d) and 100% (e).

3.5 Porosity properties

The porosities of the MOFs were determined by N_2 adsorption-desorption method after the samples were degassed at 120 °C overnight. As shown in Fig. 5A, the N_2 adsorption-desorption isotherms of the MOFs synthesized in the water/ethanol mixture with low ethanol content show a typical type I mode (curves a-c). As the ethanol volume ratio is increased to be or higher than 75%, the N_2 adsorption-desorption isotherms exhibit a mode of type IV with a pronounced adsorption-desorption hysteresis loop of type H_4, corresponding to mesoporous and microporous materials (curves b and d). The BET (Brunauer, Emmett and Teller) surface area (S_{BET}) and total pore volume (V_t) of the MOFs are listed in Table 1. Both S_{BET} and V_t values are increased with the increasing ethanol volume ratio, which can be attributed to the decreased particle size. When the ethanol volume ratio reaches to 75%, the largest S_{BET} of 1067 m^2g^{-1} and V_t of 0.52 cm^3g^{-1} were obtained. It is noteworthy that the S_{BET} and V_t values of the MOF synthesized in pure ethanol are lower than those of the MOF formed in the mixture with ethanol volume ratio of 75%. Although the MOF synthesized in pure ethanol has the smallest particle size, the aggregation of the particles (Fig. 2e) may be responsible for the dropped porosities. All the as-synthesized MOFs display the S_{BET} and V_t values higher than those of the first reported HKUST-1 (S_{BET} = 692 m^2g^{-1}, V_t = 0.33 cm^3g^{-1}),[24] except sample a.

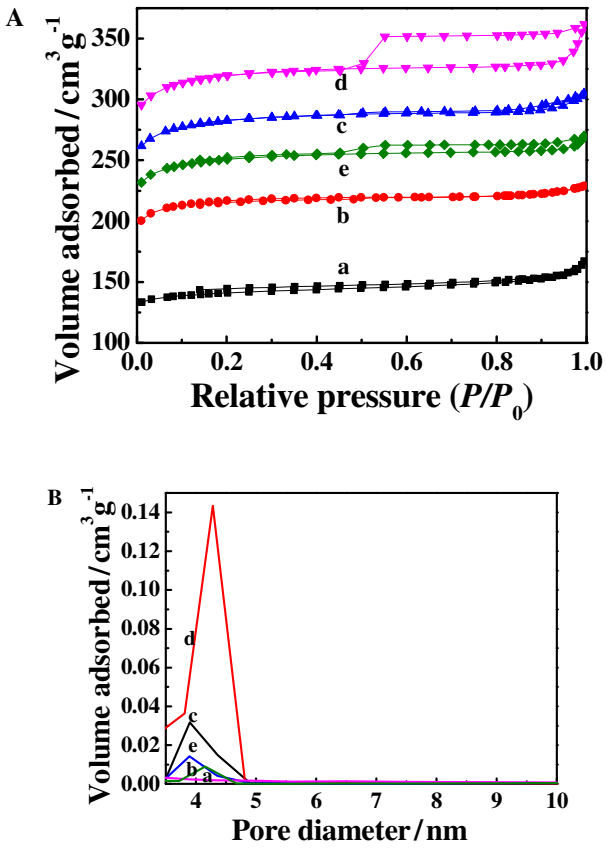

Fig. 5 N_2 adsorption-desorption isotherms (A) and mesopore size distribution (B) of the $Cu_3(BTC)_2$ synthesized in water/ethanol mixtures with ethanol volume ratios of 33% (a), 50% (b), 67% (c), 75% (d) and 100% (e).

Table 1. The average particle diameter (d), BET surface area (S_{BET}), total pore volume (V_t) and mesopore diameter (D_{meso}) of the $Cu_3(BTC)_2$ synthesized in water/ethanol mixtures with different ethanol volume ratios of 33% (a), 50% (b), 67% (c), 75% (d), and 100% (e).

Sample	d / nm	S_{BET} / m^2g^{-1}	V_t / cm^3g^{-1}	D_{meso} / nm
a	300	470	0.25	7.2
b	60	724	0.35	4.3
c	40	946	0.46	4.4
d	30	1067	0.52	4.4
e	20	837	0.40	3.9

The mesopore size distribution curves, calculated from Barrett-Joyner-Halenda analysis, are shown in Fig. 5B. The mesopore size of the five MOFs is roughly decreased with the increasing ethanol volume ratio, which can be clearly seen from Table 1. The above analysis proves that the porosity properties of the MOFs can be tuned by the easy control of ethanol volume ratio.

For comparison, the N_2 adsorption-desorption isotherms of the samples synthesized in water/ethanol mixtures with ethanol volume ratios of 0 and 25% were determined and the results are shown in Fig. S1. The S_{BET} values of the two samples are extremely low (8 m^2g^{-1} and 11 m^2g^{-1}, respectively). It can be due to the destroyed crystal structures of $Cu_3(BTC)_2$ and the loss of porous properties, which is consistent with the XRD results that $Cu_3(BTC)_2$ cannot be formed in water/ethanol mixtures with ethanol volume ratios smaller than 33%.

3.6 Intermolecular interactions

The above results reveal that the solvent properties determine the formation and properties of the as-synthesized MOF. To get information on the mechanism, the interactions between solvent molecules and the organic ligand H_3BTC were investigated by UV-vis spectra.[41,42] Fig. 6 shows the UV-vis spectra of H_3BTC dissolved in water/ethanol mixtures with different ethanol volume ratios. The maximum absorption wavelength of H_3BTC molecule is red-shifted with the increasing ethanol volume ratio, which can be clearly observed from the inset of Fig. 6. It indicates that the interactions between solvent molecules and H_3BTC molecules are weakened with the increasing ethanol content. Two reasons are responsible for this phenomenon. One reason is that the hydrogen bonding interaction between water and H_3BTC is stronger than that between ethanol and H_3BTC. Consequently, with the increasing ethanol content, the interaction between solvent molecules and H_3BTC molecules is reduced. Another reason is from the solvent itself. It has been recognized that water-alcohol molecular clusters are formed in water/ethanol mixture due to the strong hydrogen bonding interactions.[43-45] It is suggested that the strong interaction between water and ethanol molecules would weaken the interaction between water and H_3BTC molecules. The reduced interactions between solvent and H_3BTC is favorable for the coordination of organic ligand with metal ions, thus promoting the MOF formation in water/ethanol mixture as the ethanol content reaches a certain value.

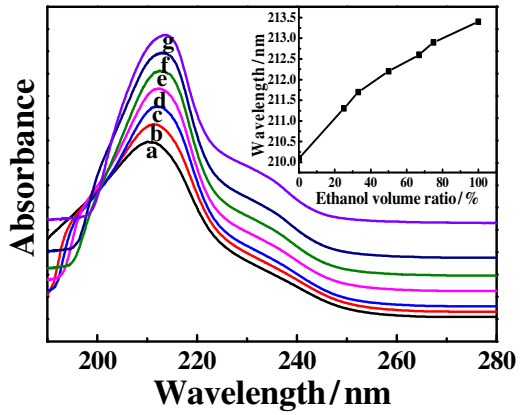

Fig. 6 UV-vis spectra of H_3BTC dissolved in water/ethanol mixtures with ethanol volume ratios: (a) 0, (b) 25%, (c) 33%, (d) 50%, (e) 67%, (f) 75% and (g) 100%. The inset describes the dependence of the maximum absorption wavelength of H_3BTC on ethanol volume ratio.

3.7 Mechanism

Based on the above results and discussion, a possible mechanism for the MOF formation and property modulation in water/ethanol mixtures is proposed in Scheme 1. With a small amount of ethanol in water, the water-ethanol clusters like $(H_2O)_mEtOH$ are formed. The massive water molecules form hydrogen bonding interactions with H_3BTC, preventing the approach of carboxylate groups to Cu(II). At this stage, the amount of ethanol is too few to influence the interactions between water molecules and ligands. As a result, Cu (II) is unable to coordinate with the organic ligand effectively and the $Cu_3(BTC)_2$ MOF cannot form (Scheme 1a). When the ethanol volume ratio reaches to 33%, more water molecules may occupy around ethanol molecules, resulting in clusters like $(H_2O)_m(EtOH)_n$. The reduced interactions between water molecules and H_3BTC guarantee that the carboxylate groups of H_3BTC coordinate to Cu(II) effectively. Therefore, $Cu_3(BTC)_2$ nanoparticles come into being (Scheme 1b). With more ethanol added into the system, most water molecules are surrounded by ethanol molecules, forming clusters in the form of $H_2O(EtOH)_n$. The coordination of H_3BTC with Cu(II) is thus greatly facilitated. The nucleation rate becomes higher, which is favorable for the formation of smaller MOF nanocrystals (Scheme 1c).

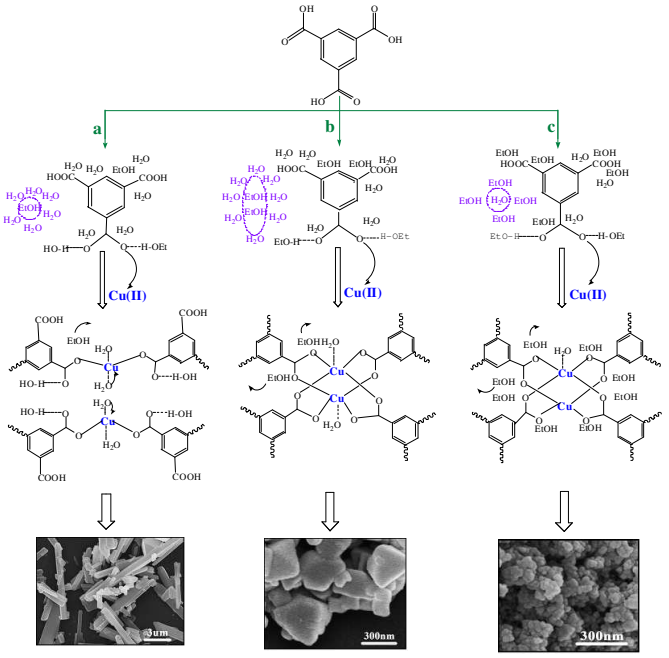

Scheme 1. Schematic illustration for the formation of $Cu_3(BTC)_2$ and modulation on particle size in water/ethanol solvent with a little ethanol (a), appropriate ethanol (b) and substantial ethanol (c).

Conclusions

In this study, we explored the formation of $Cu_3(BTC)_2$ in water/ethanol solvent systems. In absence of ethanol or with a small amount of ethanol in water, the $Cu_3(BTC)_2$ MOF cannot form. However, as the ethanol amount reaches to an enough high value (>30 vol%), the $Cu_3(BTC)_2$ MOF can be obtained in the mixed solvent at room temperature. The as-synthesized $Cu_3(BTC)_2$ crystals have average size in range of 20-300 nm, which can be adjusted through controlling the composition of the mixed solvent. It was demonstrated that the hydrogen bonding strength between solvent molecules and ligands determines the formation and properties of the $Cu_3(BTC)_2$. This work provides a new insight into the solvent effect on the MOF formation, especially meaningful for the synthesis of water-sensitive MOF in an aqueous medium. We hope that more wide researches on adjusting the self-assemblies of MOFs by varying the solvent properties will be triggered in future.

Acknowledgements

We thank the National Natural Science Foundation of China (21173238, 21133009, U1232203, 21321063), Chinese Academy of Sciences (KJCX2.YW.H16).

Notes and references

Beijing National Laboratory for Molecular Sciences, Key Laboratory of Colloid and Interface and Thermodynamics, Institute of Chemistry, Chinese Academy of Sciences, Fax: 86-10-62559373; Tel: 86-10-62562821; E-mail: zhangjl@iccas.ac.cn

1 J. J. Goings, S. M. Ohlsen, K. M. Blaisdell and D. P. Schofield, *J. Phys. Chem. A*, 2014, **118**, 7411.

2 S. Q. Ma, D. F. Sun, J. M. Simmons, C. D. Collier, D. Q. Yuan and H. C. Zhou, *J. Am. Chem. Soc.*, 2008, **130**, 1012.
3 H. Furukawa, N. Ko, Y. B. Go, N. Aratani, S. B. Choi, E. Choi, A. O. Yazaydin, R. Q. Snurr, M. O'Keeffe and J. Kim, *Science*, 2010, **329**, 424.
4 T. Rodenas, I. Luz, G. Prieto, B. Seoane, H. Miro, A. Corma, F. Kapteijn, F. X. L. I. Xamena and J. Gascon, *Nat. Mater.*, 2015, **14**, 48.
5 K. M. L. Taylor-Pashow, J. Della Rocca, Z. G. Xie, S. Tran and W. B. Lin, *J. Am. Chem. Soc.*, 2009, **131**, 14261.
6 W. J. Rieter, K. M. Pott, K. M. L. Taylor and W. B. Lin, *J. Am. Chem. Soc.*, 2008, **130**, 11584.
7 L. E. Kreno, K. Leong, O. K. Farha, M. Allendorf, R. P. Van Duyne and J. T. Hupp, *Chem. Rev.*, 2012, **112**, 1105.
8 L. Peng, J. L. Zhang, Z. M. Xue, B. X. Han, X. X. Sang, C. C. Liu and G. Y. Yang, *Nat. Commun.*, 2014, **5**, 5465.
9 A. Corma, H. Garcia and F. X. L. I. Xamena, *Chem. Rev.*, 2010, **110**, 4606.
10 J. Lee, O. K. Farha, J. Roberts, K. A. Scheidt, S. T. Nguyen and J. T. Hupp, *Chem. Soc. Rev.*, 2009, **38**, 1450.
11 Y. F. Yue, Z. A. Qiao, P. F. Fulvio, A. J. Binder, C. C. Tian, J. H. Chen, K. M. Nelson, X. Zhu and S. Dai, *J. Am. Chem. Soc.*, 2013, **135**, 9572.
12 X. R. Hao, X. L. Wang, K. Z. Shao, G. S. Yang, Z. M. Su and G. Yuan, *CrystEngComm.*, 2012, **14**, 5596.
13 X. Zhou, P. Liu, W. H. Huang, M. Kang, Y. Y. Wang and Q. Z. Shi, *CrystEngComm.*, 2013, **15**, 8125.
14 H. Q. Du, J. F. Bai, C. Y. Zuo, Z. F. Xin and J. B. Hu, *CrystEngComm.*, 2011, **13**, 3314.
15 S. R. Bajpe, C. E. A. Kirschhock and A. Aerts, *Chem. −Eur. J.*, 2010, **16**, 3926.
16 Z. M. Xue, J. L. Zhang, L. Peng, B. X. Han, T. C. Mu, J. S. Li and G. Y. Yang, *ChemPhysChem.*, 2014, **15**, 85.
17 H. L. Guo, Y. Z. Zhu, S. Wang, S. Q. Su, L. Zhou and H. J. Zhang, *Chem. Mater.*, 2012, **24**, 444.
18 W. J. Son, J. Kim, J. Kim and W. S. Ahn, *Chem. Commun.*, 2008, **47**, 6336.
19 J. Y. Ye and C. J. Liu, *Chem. Commun.*, 2011, **47**, 2167.
20 X. Q. Cheng, A. F. Zhang, K. K. Hou, M. Liu, Y. X. Wang, C. S. Song, G. L. Zhang and X. W. Guo, *Dalton Trans.*, 2013, **42**, 13698.
21 C. Y. Sun, S. X. Liu, D. D. Liang, K. Z. Shao, Y. H. Ren and Z. M. Su, *J. Am. Chem. Soc.*, 2009, **131**, 1883.
22 Y. Qi, F. Luo, Y. X. Che and J. M. Zhen, *Cryst. Growth Des.*, 2008, **2**, 606.
23 N. ul Qadir, S. A. M. Said and H. M. Bahaidarah, *Microporous Mesoporous Mater.*, 2014, **201**, 61.
24 S. S. Y. Chui, S. M. F. Lo, J. P. H. Charmant, A. G. Orpen, I. D. Williams, *Science*, 1999, **283**, 1148.
25 S. Xiang, W. Zhou, J. M. Gallegos, Y. Liu and B. Chen, *J. Am. Chem. Soc.*, 2009, **131**, 12415.
26 M. H. Pham, G. T. Vuong, F. G. Fontaine and T. O. Do, *Cryst. Growth Des.*, 2012, **12**, 1008.
27 L. B. Sun, J. R. Li, J. Park and H. C. Zhou, *J. Am. Chem. Soc.*, 2012, **134**, 126.
28 Y. Wu, F. Li, W. Zhu, J. Cui, C. Tao, C. Lin, P. M. Hannam and G. Li, *Angew. Chem., Int. Ed.*, 2011, **50**, 12518.
29 C. Carbonell, I. Imaz and D. Maspoch, *J. Am. Chem. Soc.*, 2011, **133**, 2144.
30 E. Soubeyrand-Lenoir, C. Vagner, J. W. Yoon, P. Bazin, F. Ragon, Y. K. Hwang, C. Serre, J. S. Chang and P. L. Llewellyn, *J. Am. Chem. Soc.*, 2012, **134**, 10174.
31 R. Ameloot, F. Vermoortele, J. Hofkens, F. C. D. Schryver, D. E. De Vos and M. B. J. Roeffaers, *Angew. Chem., Int. Ed.*, 2013, **52**, 401.
32 G. Majano, O. Martin, M. Hammes, S. Smeets, C. Baerlocher and J. Perez-Ramirez, *Adv. Funct. Mater.*, 2014, **24**, 3855.
33 J. J. Low, A. I.Benin, P. Jakubczak, J. F. Abrahamian, S. A. Faheem and R. R. Willis, *J. Am. Chem. Soc.*, 2009, **131**, 15834.
34 Y. J. Zhao, J. L. Zhang, B. X. Han, J. L. Song, J. S. Li and Q. A. Wang, *Angew. Chem., Int. Ed.*, 2011, **50**, 636.
35 H. X. Guo, F. Lin, J. H. Chen, F. M. Li and W. Weng, *Appl. Organometal. Chem.*, 2015, **29**, 12.
36 K. L. Zhang, F. Zhou, L. M. Yuan, G. W. Diao and S. W. Ng, *Inorg. Chim., Acta*, 2009, **362**, 2510.
37 P. X. Chen, G. P. Yang, L. Hou, Y. Y. Wang and Q. Z. Shi, *J. Coord. Chem.*, 2012, **65**, 2893.
38 L. Peng, J. L. Zhang, J. S. Li, B. X. Han, Z. M. Xue and G. Y. Yang, *Chem. Commun.*, 2012, **48**, 8688.
39 K. L. Zhang, W. Liang, Y. Chang, L. M. Yuan and S. W. Ng, *Polyhedron*, 2009, **28**, 647.
40 H. W. Yang, S. Orefuwa and A. Goudy, *Microporous Mesoporous Mater.*, 2011, **143**, 37.
41 I. Bolz and S. Spange, *Chem. −Eur. J.*, 2008, **14**, 9338.
42 J. L. Zhang, B. X. Han, Y. J. Zhao, J. S. Li and G. Y. Yang, *Chem. −Eur. J.*, 2011, **17**, 4266.
43 S. Dixit, J. Crain, W. C. K. Poon, J. L. Finney and A. K. Soper, *Nature*, 2002, **416**, 829.
44 E. J. W. Wensink, A. C. Hoffmann, P. J. van Maaren and D. van der Spoel, *J. Chem. Phys.*, 2003, **119**, 7308.
45 A. Wakisaka and K. Matsuura, *J. Mol. Liq.*, 2006, **129**, 25.

